Nanoscale Res Lett (2010) 5:469–477
DOI 10.1007/s11671-009-9516-2

SPECIAL ISSUE ARTICLE

On the Chemical Origin of the Gap Bowing in $(GaAs)_{1-x}Ge_{2x}$ Alloys: A Combined DFT–QS*GW* Study

Giacomo Giorgi · Mark Van Schilfgaarde · Anatoli Korkin · Koichi Yamashita

Received: 20 November 2009 / Accepted: 17 December 2009 / Published online: 7 January 2010
© The Author(s) 2010. This article is published with open access at Springerlink.com

Abstract Motivated by the research and analysis of new materials for photovoltaics and by the possibility of tailoring their optical properties for improved solar energy conversion, we have focused our attention on the $(GaAs)_{1-x}Ge_{2x}$ series of alloys. We have investigated the structural properties of some $(GaAs)_{1-x}Ge_{2x}$ compounds within the local-density approximation to density-functional theory, and their optical properties within the Quasiparticle Self-consistent *GW* approximation. The QS*GW* results confirm the experimental evidence of asymmetric bandgap bowing. It is explained in terms of violations of the octet rule, as well as in terms of the order–disorder phase transition.

Keywords Photovoltaics · III–V IV-doped alloys · Bandgap bowing · Order–disorder phase transition · DFT · Quasiparticle Self-consistent *GW*

Introduction

The design of semiconductors with controlled bandgaps E_G, unit cell parameters, and low defect concentration is the ultimate aim in several important areas of industrial applications—electronics, photonics, light-emitting devices, and photovoltaics (PV). Efficient collection of solar energy requires materials that absorb light from different portions of the solar spectrum, followed by efficient conversion into electrons and holes at *p–n* junctions. A natural approach to the design of new semiconductors is to alloy two materials with similar lattice parameters but different bandgaps. For example, Ge ($E_G = 0.67$ eV [1] at 300 K) and GaAs ($E_G = 1.43$ eV [1] at 300 K) have very similar lattice parameters, 5.649 and 5.66 Å, respectively [2, 3]. There is thus the appealing possibility that $(GaAs)_{1-x}Ge_{2x}$ alloys with intermediate bandgaps can be realized, in particular one characterized by a direct gap, $1 < E_G < 1.4$ eV (i.e., the average between the bandgaps of Ge and GaAs), which corresponds to the maximum efficiency solar cell for a single bandgap material [4]. Indeed, several theoretical [5–12] and experimental [13–18] papers have been published on studies of metastable alloys between III–V and IV group semiconductors, formally $(III–V)_{1-x}(IV)_{2x}$ compounds.

A group of such mixed single crystal metastable semiconductors covering a wide composition range was synthesized by vapor phase deposition techniques. Noreika et al. [17] deposited $(GaAs)_{1-x}Si_x$ on GaAs(111) by the reactive *rf* sputtering technique, and they reported an optical bandgap at room temperature of about 1.28 eV for $(GaAs)_{0.45}Si_{0.55}$. Baker et al. [18] measured the Raman spectra of $(GaSb)_{1-x}Ge_x$ alloys, and found both GaSb- and Ge-like optical modes. The Ge-like mode frequency depends on the alloy's composition within about 40 cm^{-1}, whereas the GaSb-like mode does not.

(III–V)–IV alloys such as $(GaAs)_{1-x}Ge_{2x}$, characteristically display a large negative, V-shaped bowing of E_G as a function of the alloy composition x. A minimum value of $\sim$0.5 eV was detected by Barnett et al. [13] at a Ge concentration of about 35%, corresponding to the critical value (x_c) for phase transition between an ordered zincblende (ZB) and a disordered diamond structure. In the ordered

G. Giorgi (✉) · K. Yamashita
Department of Chemical System Engineering,
School of Engineering, University of Tokyo,
Tokyo 113-8656, Japan
e-mail: giacomo@tcl.t.u-tokyo.ac.jp

M. Van Schilfgaarde · A. Korkin
Arizona State University, Tempe, AZ 85287, USA

GaAs-rich phase, Ga and As preferentially form donor–acceptor pairs, whereas in the Ge-rich phase, they are randomly distributed in the alloy forming a mixture of *n*-type (As in Ge) and *p*-type (Ga in Ge) semiconductors. This phase transition has been put forward to explain [19] the large bowing. Several models have been developed for the ZB → diamond phase transition [8, 19–26]. The stochastic model by Kim and Stern [22] well reproduces this phase transition along the <100> direction at $x_c = 0.3$. However, it poorly describes the growth along the <111> direction, with accumulation of Ge on alternate {111} planes. In general, kinetic models seem to be more appropriate descriptors of the ZB—diamond phase transition than thermodynamic ones: the latter do not take into account the nonuniqueness of the critical composition x_c as a function of kinetic growth; they require as input the critical concentration at which the transition takes place, but no restrictions on the formation of Ga–Ga and As–As bonds are imposed. Other models based on the percolation method [26] lead to ZB → diamond transition at $x_c = 0.57$; percolation theory also does not account for different growth conditions. Rodriguez et al. [8] reported that the growth direction and avoidance of "bad bond" formation (i.e., Ga–Ga and As–As bonds) (long-range order, *LRO*) effects are the main factors responsible for atomic ordering in $(GaAs)_{1-x}Ge_{2x}$ alloys. According to the same model, E_G is influenced only by nearest neighbor (*NN*) atomic interactions (short-range order, *SRO*) effects. In an extension of the stochastic model of growth along the <100> direction, Holloway and Davis [23, 24] formulated a model for alloys grown in the <100> and <111> directions. SRO effects are common for these two directions. In contrast, the impact of LRO is quite different: a tendency to convert to <111> As growth is predicted [24] as a consequence of the instability of the growth in the <111> Ga direction. In a previous paper [25], the same authors note that the transition from ZB to diamond does not affect the energy gap of $(GaAs)_{1-x}Ge_{2x}$: this model predicts a critical concentration for the order–disorder transition with $x_c = 0.75$, without any dependence on the method of growth. SRO and LRO effects on the electronic properties of many other IV-doped III–V alloys have also been compared by combining the special quasirandom structures (SQS) and the simulated-annealing (SA) methods for cells of various sizes in conjunction with an empirical pseudopotential approach [27]. In particular, the direct bandgaps of ideal random $Al_{1-x}Ga_xAs$, $Ga_{1-x}In_xP$, and $Al_{1-x}In_xAs$ alloys were studied. SRO effects are reported to increase the optical bowing of the direct bandgap.

Surface faceting has also been detected in these systems, reported to take place with a subsequent phase separation between the GaAs-rich ZB and Ge-rich diamond region during the growth on (001)-oriented GaAs substrates [15]. A direct consequence attributable to the faceting is the bandgap narrowing of such $(GaAs)_{1-x}Ge_{2x}$ $(0 < x < 0.22)$ alloy layers grown by low-pressure metal–organic vapor phase epitaxy. A similar phenomenon has been reported only once previously, for $InAs_ySb_{1-y}$ grown by molecular beam epitaxy grown at low temperature (T_g) [28]. It has been also demonstrated that growth temperature [16] strongly affects the nature of the alloy. $(GaAs)_{1-x}Ge_{2x}$ layers have been epitaxially grown on GaAs (100) substrates at different temperatures. Transmission electron microscopy analysis revealed that at $T_g = 550°C$, Ge separated from GaAs into domains of ~100 Å. Single-phase alloys are detected differently at $T = 430°C$.

In spite of considerable recent research in novel complex materials for photovoltaics, the relationship between chemical and optical properties of III–V–IV alloys and similar materials is still unknown, and is a matter of current debate. In the present paper, we investigate the chemical nature of the bowing in $(GaAs)_{1-x}Ge_{2x}$ alloys. In particular, we theoretically investigated the structural and optical properties of four different intermediate structured compounds that range between "pure" GaAs and "pure" Ge ($x_{Ge} = 0.25$, 0.50 (two samples), 0.75).

Computational Details

We performed calculations by using density-functional theory (DFT), within both the local-density approximation (LDA) [29, 30] and the generalized gradient approximation (GGA) of Perdew and Wang [31–33]. We used Blöchl's all-electron projector-augmented wave (PAW) method [34, 35], with PAW potentials with *d* electrons in the semicore for both Ga and Ge. Cutoff energies of 287 and 581 eV were set as the expansion and augmentation charge of the plane wave basis. The force convergence criterion for these models was 0.01 eV/Å. The initial $(GaAs)_{1-x}Ge_{2x}$ models consisting of eight atoms were optimized with a 10^3 Γ-centered *k*-points sampling scheme.

All the total energy calculations were also performed with the generalized full-potential LMTO method of Ref. [36]. Calculated structural properties and heats of reaction predicted by the two methods were almost identical, indicating that the results are well converged.

The thermodynamic stability of these alloys was calculated as the ΔE products–reactants of the equation:

$$GaAs + 2xGe \rightarrow (GaAs)_{1-x}Ge_{2x} + xGaAs. \quad (1)$$

It is expected that LDA and GGA predict reasonable heats of reaction of the type in Eq. 1, since reactions involve rearrangement of atoms on a fixed (zincblende) lattice, and there is a large cancelation of errors. Optical properties are

much less well described. The LDA is well known to underestimate semiconductor bandgaps, and moreover, the dispersion in the conduction band is poor. In Ge, the LDA gap is negative and Γ_{1c} is lower than L_{1c} in contradiction to experiment. Also the Γ-X dispersion is often strongly at variance with experiment: in GaAs X_{1c}–Γ_{1c} is about twice the experimental value of 0.48 eV.

When considering $(GaAs)_{1-x}Ge_{2x}$ alloys, any of the three points (Γ, X, L) may turn out to be minimum-gap points, so all must be accurately described. Thus, the LDA is not a suitable vehicle for predicting optical properties of these structures.

It is widely recognized that the *GW* approximation of Hedin [37] is a much better predictor of semiconductor optical properties. The *GW* approximation is a perturbation theory around some noninteracting Hamiltonian H_0; thus the quality of the *GW* result depends on the quality of H_0. It is also important to mention that for reliable results, care must be taken to use an all-electron method [38]. We adopt here a particularly reliable all-electron method, where not only the eigenfunctions are expanded in an augmented wave scheme, but the screened coulomb interaction W and the self-energy $\Sigma = iGW$ are represented in a mixed plane wave and molecular orbital basis [39, 40]. All core states are treated at the Hartree–Fock level.

GW calculations in the literature usually take H_0 from the LDA; thus, we may call this the $G^{\mathrm{LDA}}W^{\mathrm{LDA}}$ approximation. There are many limitations to $G^{\mathrm{LDA}}W^{\mathrm{LDA}}$; see e.g., Ref. [41]. In particular, the $G^{\mathrm{LDA}}W^{\mathrm{LDA}}$ gap for GaAs is 1.33 eV. The Quasiparticle Self-consistent *GW* (QS*GW*) approximation, recently developed by one of us [42], overcomes most of these limitations. Semiconductor energy band structures are well described with uniform reliability. Discrepancies with experimental semiconductor bandgaps are small and highly systematic (e.g., $E_g^{\mathrm{QS}GW} \approx E_g^{\mathrm{expt}} + 0.25\,\mathrm{eV}$ for most semiconductors [41]), and the origin of the error can be explained in terms of ladder diagrams missing in the random phase approximation (RPA) to the polarizability $\Pi(\mathbf{r},\mathbf{r}',\omega)$ [43]. While standard QS*GW* would be sufficient for this work, we can do a little better by exploiting our knowledge of the small errors originating from the missing vertex in Π. In principle ladder diagrams can be included explicitly via the Bethe–Salpeter equation, but it is very challenging to do. It has never been done in the QS*GW* context except in a very approximate manner [43]. On the other hand, in *sp* semiconductors, the consequences of this vertex are well understood. The RPA results in a systematic tendency for the dielectric constant, ε_∞, to be underestimated. The error is very systematic: to a very good approximation ε_∞ is too small by a *universal* factor of 0.8, for a wide range of semiconductors and insulators [44]. This fact, and the fact that quasiparticle excitations are predominantly controlled by the static limit of W, provides a simple and approximate remedy to correct this error: we scale Σ (more precisely $\Sigma - V_{xc}^{\mathrm{LDA}}$) by 0.8. While such a postprocessing procedure is admittedly *ad hoc*, the basis for it is well understood and the scaling results in a very accurate ab initio scheme for determining energy band structures (to within $\sim$0.1 eV when the effect of zero-point motion on bandgaps is taken into account) and effective masses for essentially any semiconductor. Here, we adopt this scaling procedure to refine our results to this precision. In any case corrections are small, and our conclusions do not depend in any way on this scaling. Results for GaAs and Ge are shown in Table 1.

Results

We performed preliminary calculations at the DFT level of GaAs and Ge; Table 2 lists the main structural optimized parameters of the two most stable polymorphs of GaAs, zincblende (ZB, group 216, *F-43m*, $Z = 4$) and wurtzite (WZ, group 186, *P63mc*, $Z = 2$) and of Ge in its cubic form (group 227, *Fd-3m*, $Z = 8$).

As seen from Table 2, the LDA generates structural properties closer to experiment than GGA in this context.

Table 1 Left, LDA calculated bandgaps (LMTO [36], Spin–Orbit effects included) for Γ, X, L points for GaAs and Ge Right, QS*GW* bandgaps for the same points in Ge and GaAs (eV, 0 K), compared with measured values at 0 K. The self-energy was scaled by a factor 0.8, as described in the text. Raw (unscaled) QS*GW* levels are slightly larger than experiment

	LDA BANDGAP (eV)			QS*GW* BANDGAP (eV)					
	Γ	L	X	Γ		L		X	
				QS *GW*	Exp	QS *GW*	Exp	QS *GW*	Exp
GaAs (dir.)	0.23	0.75	1.43	1.47	1.52[a]	1.73	1.80[a]	1.84	1.98[a]
Ge (indir)	−0.22	−0.04	0.55	0.94	0.90[b]	0.74	0.74[b]	1.06	1.09[b]

[a] Inferred from ellipsometry data in Ref. [45], using the QS*GW* Γ-X dispersion in the valence band (−3.37 eV)

[b] Inferred from ellipsometry data in Ref. [46], using the QS*GW* Γ-X dispersion in the valence band (−3.98 eV)

Table 2 The energy difference (ΔE, per unit, eV) between ZB and WZ polymorphs of GaAs, lattice constant, a, and bulk moduli B (GPa) of GaAs (ZB) and Ge (diamond)

	GaAs (ZB) 216, F-$43m$, $Z = 4$	GaAs (WZ) 186, $P63mc$, $Z = 2$	Ge (cubic) 227, Fd-$3m$, $Z = 8$
This study, PAW/LDA			
ΔE	–	+0.06	–
B	66.14		71.8
Lattice constant (Å)	$a = 5.605$	$a = 3.917$, $b = 3.886$ $c = 6.505$	$a = 5.612$
This study, PAW/GGA			
ΔE	–	+0.03	–
B	79.01		71.0
Lattice constant (Å)	$a = 5.739$	$a = 4.040$, $c = 6.668$	$a = 5.747$
Previous study (LDA)			
ΔE	–	+0.0120[a]	
B	75.7[b], 77.1[e]		73.3[c], 79.4[c]
Lattice constant (Å)	$a = 5.654$[a], 5.53[b] 5.508[e], 5.644[k]	$a = 3.912$, $c = 6.441$[a] $a = 3.912$, $c = 6.407$[b]	$a = 5.58$[c], 5.53[c]
Previous study (GGA)			
B	59.96[h]		55.9[c]
Lattice constant (Å)	$a = 5.74$[h], 5.722[i]	$a = 3.540$, $c = 6.308$[l]	$a = 5.78$[c]
Experimentally			
ΔE	–	+0.0117[k]	
B	77[f]		75[d]
Lattice constant (Å)	$a = 5.649$[f], 5.65[g]		$a = 5.678$[j], 5.66[d]

[a] Ref. [47], [b] Ref. [3], [c] Ref. [48], [d] Ref. [2], [e] Ref. [49], [f] Ref. [50], [g] Ref. [51] [h] Ref. [52], [i] Ref. [53], [j] Ref. [54], [k] Ref. [55], [l] Ref. [56]

Thus, we use LDA to study structural properties. Both Ga–As and Ge–Ge bond lengths are 2.43 Å in their most stable polymorph.

ZB–GaAs is constituted by interpenetrating fcc sublattices of cations (Ga) and anions (As). The diamond lattice of Ge may be thought of as the ZB structure with Ge occupying both cation and anion sites. Here, we consider 8-atom $(GaAs)_{1-x}Ge_{2x}$ compounds that vary the Ge composition, including pure GaAs ($x = 0$) to $x = 0.25$ (2 Ge atoms), $x = 0.50$ (4 Ge atoms), $x = 0.75$ (6 Ge atoms) (see Fig. 1), and finally pure Ge ($x = 1$).

At first, we performed an analysis of the Ge dimer in bulk GaAs, at site positions (1/4, 1/4,1/2) and (0,1/2,3/4). We denote this as "alloy model **I**", the dimer in an 8-atom GaAs cell with lattice vectors (100), (010), and (001) before relaxation. It can be considered a highly concentrated molecular substitutional Ge_2 defect in GaAs, for which we predict stability owing to the donor–acceptor self-passivation mechanism.[1] The first layer of **I** consists only of As; the second and the third layers (along [001]), are Ge–Ga, and Ge–As, respectively. The fourth is pure Ga. Then, the overall sequence is a repeated "sandwich-like" structure, ···/As/Ge–Ga/Ge–As/Ga/···. The bond lengths were calculated to be 2.38 (Ga–Ge), 2.42 (Ge–Ge), 2.44 (Ga–As), and 2.47 Å (Ge–As)—relatively small variations around the calculated values in bulk Ge and GaAs (2.43 Å). This is perhaps not surprising as the electronic structure can roughly be described in terms of nearly covalent two-center bonds [electronegativity $\chi = 1.81$, 2.01, and 2.18, for Ga, Ge, and As, respectively (http://www.webelements.com)]. In the alloy **I** the number of "bad bonds" [7, 8], i.e., the number of III–IV and IV–V nearest neighbors, is 12, or 37.5% of the total. According to the Bader analysis [57–59], in the pure host, the difference in electronegativity is responsible for charge transfer from cation to anion. In the alloy formation process, the introduction of Ge reduces the ionic character of the GaAs bond, while increasing the ionic character of the Ge–Ge bond. When a Ge dimer is inserted in GaAs, 0.32 electrons are transferred away from Ge_{Ga} site, while Ge_{As} gains 0.21 electrons The charge deficit on Ga, is reduced from 0.6 electrons in bulk GaAs to 0.47e, while the charge excess on As is reduced from 0.6 to 0.5e. ΔE for reaction Eq. (1) was 0.55 eV, and the optimized lattice parameter was $a = 5.621$ Å. We have also considered Ge donors (Ge_{Ga}) and acceptors (Ge_{As}) in the pure 8-atom GaAs host cell,

[1] We preliminarily performed calculations on the stability of substitutional Ge donor (Ge_{Ga}), acceptor (Ge_{As}), and Ge pairs in GaAs. We have both compared the stability of Ge_2 molecule and 2Ge isolated in a 64-atom supercell GaAs host. Similarly, we calculated the stability of As_{Ge}, Ga_{Ge}, and $GaAs_{Ge2}$ still in a 64-atom supercell Ge host. For sake of consistency, these calculations were performed at the same level of theory of present calculations (PAW/LDA), with same cutoff, reduced k-point sampling (4^3 Γ-centered), and force convergence threshold which is reduced up to 0.05 eV/Å.

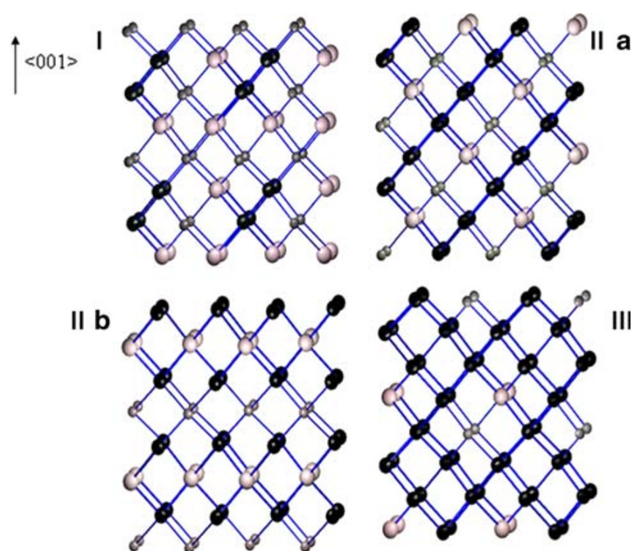

Fig. 1 Four $(GaAs)_{1-x}Ge_{2x}$ models investigated. [Ga, *small gray*; As, *large white*; Ge, *large black*]

separately. The formation energy has been computed according to the Zhang–Northrup formalism [60]. In particular, we calculate ΔE to be 1.03 eV for Ge_{Ga} and 0.84 for Ge_{As}. The sum of the single contributions (1.87 eV) is larger than the heat of formation of the dimer, structure **I** (0.55 eV). Two reasons explain this difference in energy. First, in the **I** model alloy, at least one correct bond III–V is formed while in the separate Ge_{Ga} (IV–V) and Ge_{As} (IV–III) cases only bad bonds are formed. The isolated Ge_{Ga} is a donor; the isolated Ge_{As} is an acceptor. Neither is stable in their neutral charged state. We have tested it in a previous analysis (see Footnote) where we calculated +1 and −1 as the most stable charged state for Ge_{Ga} and Ge_{As}, for almost the range of the electronic chemical potential, μ_e. These two charged states are indeed formally isoelectronic with the host GaAs. That the stabilization energy 1.87–0.55 = 1.33 eV is only slightly smaller than the host GaAs bandgap establishes that the pair is stabilized by a self-passivating donor–acceptor mechanism.

We considered two alternative structures for the $x_{Ge} = 0.50$ case. In the **IIa** structure, Ge atoms are substituted for host atoms at (1/2, 0, 1/2), (1/2, 1/2, 0), (3/4, 3/4, 1/4), and (3/4, 1/4, 3/4); then the lattice was relaxed. It results in a stacking ···/Ga–Ge/Ge–As/··· along <001>. The three cubic directions are no longer symmetry-equivalent: the optimized lattice parameters were found to be $a = 5.590$ Å, $b = c = 5.643$ Å. The four intralayer bond lengths were calculated to be Ga–Ge (2.39 Å), Ge–As (2.48 Å), Ge–Ge (2.42 Å), and Ga–As (2.44). Because of the increased amount of Ge, structure **IIa** was less polarized than **I**, as confirmed by the slightly more uniform bond lengths. In **IIa** alloy, the number of "bad bonds" is 16 (i.e., 50%) and ΔE rises to 0.72 eV. In the **IIb** structure, Ge atoms are substituted for host atoms at (1/4, 1/4, 1/4), (1/4, 3/4, 3/4), (3/4, 3/4, 1/4), and (3/4, 1/4, 3/4). This structure consists of a stack of pure atomic layers, ···/Ga/Ge/As/Ge···, and thus it contains *only* nearest neighbors of the (Ga–Ge) and (Ge–As) type: thus *all* bonds are "bad bonds" in this **IIb** compound. Bond lengths were calculated to be 2.40 Å and 2.49 Å, respectively, and optimized lattice parameters were $a = c = 5.682$, $b = 5.560$ Å. In this structure, $\Delta E = 1.40$ eV, almost double that of **IIa** with identical composition. It supports the picture [7, 8] that III–IV and IV–V bonds are less stable than their III–V, IV–IV counterparts.

This result confirmed findings of an analysis of the substitutional defect Ge in GaAs (see Footnote). In that case, we checked the stability of Ge_2 dimers (donor–acceptor pair formation) versus isolated Ge couples (*n*-type Ge + *p*-type Ge) in GaAs matrix in GaAs supercells. We calculate the energy reaction Ge_2:GaAs → Ge_{Ga}:-GaAs + Ge_{As}:GaAs to be positive, with $\Delta E = 0.39$ eV, and interpret this as the gain of one III–IV (Ga–Ge) and one IV–V (Ge–As) bond and the loss of one IV–IV (Ge–Ge) bond. (Note that the **IIb** structure corresponds to the high concentration limit of isolated couples.) According to phase transition theory, the symmetry lowering for the two intermediate systems is the fingerprint of an ordered–disordered phase transition [61]. The calculated deviation from the ideal cubic case ($c/a = 1$) is 0.94 and 2.15% for **IIa** and **IIb** models, respectively, confirming energetic instability for the **IIb** alloy.

The last model, **III**, [Ge] = 0.75, consists of pure Ge except that Ga is substituted at (0, 0, 0) and As at (1/4,1/4,1/4). The calculated bond lengths were 2.39, 2.43, 2.45, and 2.48 Å for Ga–Ge, Ge–Ge, Ga–As, and Ge–As, respectively. Cubic symmetry is restored: the optimized lattice parameter ($a = 5.624$ Å) is nearly identical to structure **I**. Similarly, ΔE is almost the same as **I** (~0.54 eV). Indeed, **I** and **III** are formally the same model with the same concentration (25%) of Ge in GaAs (**I**) and GaAs in Ge (**III**) and the same number of bad bonds, 12. By analogy to model **I,** we have also calculated the formation energy of a single substituted Ge in the cell. We have also made a preliminary calculation of the stability of isolated Ga acceptors (Ga_{Ge}) and As donors (As_{Ge}) versus that of the substitutional molecular $GaAs_{Ge2}$ in Ge pure host (a supercell of 64 atoms see Footnote); for such concentrations ($x_{GaAs} = 0.0312 = 1/32$ and $x_{Ga(As)} = 0.0156 = 1/64$), the molecular substitutional $GaAs_{Ge2}$ is only stabilized by 0.057 eV with respect to the separate couple acceptor–donor. This small stabilization for $GaAs_{Ge2}$ compared to isolated Ga_{Ge} and As_{Ge} confirms the expected similar probability of finding a mixture of *n*-type and *p*-type semiconductors in the "disordered" Ge-rich phase. For reference states needed to balance a reaction, we used

the most stable polymorph, of the elemental compounds i.e., orthorhombic Ga and rhombohedral As [62]. Ga-rich and As-rich conditions have been considered, corresponding to $\mu_{Ga(As)} = \mu^{bulk}_{Ga(As)}$, respectively. In the case of the 8-atom cells, the formation energy for Ga_{Ge} and As_{Ge} are 0.26 eV and 0.58 eV, respectively. Thus, the model **III** alloy stabilizes the isolated III and V substitutionals by 0.30 eV ($\Delta E(Ga_{Ge}) + \Delta E(As_{Ge}) - \Delta E_{\mathbf{III}}$). This energy is 0.4 eV less than the host bandgap, indicating that the stabilization energy is a little more complicated than a simple self-passivating donor–acceptor mechanism, as we found for the Ge molecule in GaAs.

Collecting ΔE for the different systems containing equal numbers of Ge cations and anions, we find an almost exactly linear relationship between ΔE and the number of bad bonds, as Fig. 2 shows. This striking result confirms that the electronic structure of these compounds is largely described in terms of independent two-center bonds. For stoichiometric compounds, it suggests an elementary model Hamiltonian for the energetics of any alloy with equal numbers of Ge cations and anions: $\Delta E = 0.54$, 0.72, 1.40 eV for $N = 12$, 16, 32, respectively, where N is the number of bad bonds.

Even if small variations are expected in the lattice parameter of the alloys, the Vegard's law:

$$a_{(GaAs)1-xGe2x} = xa_{Ge} + (1-x)a_{GaAs} \quad (2)$$

where $a_{(GaAs)1-xGe2x}$, a_{Ge}, a_{GaAs} are the lattice parameters of the final alloy and its components, respectively, represents a useful tool for predicting a trend in terms of lattice parameter variation for our alloy models. We have thus tested the predicted versus calculated values for the lattice parameter. In particular, for models **I** and **III**, we have used the calculated lattice parameters, a (LDA). On the other hand, since for the reduced-symmetry models **IIa** and **IIb** is $a \neq b = c$ and $a = c \neq b$, respectively, we have approximated the lattice parameter as the cubic root of the volume of each of the $x_{Ge} = 0.5$ cell models. Table 3 reports the experimental, theoretically predicted, and calculated (LDA) lattice parameters, based on Vegard's Law. These values showed the almost perfect matching between GaAs and Ge lattice parameter and at the same time the marked deviation of model **IIb** from the trend, thus confirming the main contribution of "bad bonds" to the final instability of the alloy.

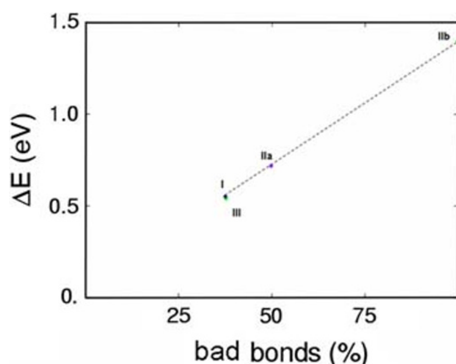

Fig. 2 Heat of formation (ΔE) of the alloy models versus the number of "bad bonds"

Table 3 Lattice parameters: a_{exp} obtained by Eq. (2) using experimental lattice parameters; a_{theor} calculated from Eq. (2), but with optimized lattice parameters at the PAW/LDA level for Ge and GaAs; a_{calc} the PAW/LDA optimized lattice parameters for models **I**, **IIa**, **IIb**, and **III**. (*Italic* is for values extrapolated as $\sqrt[3]{V}$.)

	a_{exp}	a_{theor}	$a_{calc\ (PAW/LDA)}$
GaAs	5.649[a]	5.605	
I	5.651	5.607	5.621
IIa	5.653	5.609	*5.625*
IIb			*5.641*
III	5.655	5.610	5.624
Ge	5.660[b]	5.610	

[a] From Ref. [51], [b] From Ref. [2]

We have performed QS*GW* calculations on the optimized structures (**I**, **IIa**, **IIb**, and **III**) and also for the pure GaAs and Ge 8-atom cells. Table 4 shows the QS*GW* bandgaps for the Γ and R points. In Fig. 3, we report the electronic structure for all the models considered (pure GaAs, Ge, and the intermediate alloy models). In the simple cubic supercell, R corresponds to L of the original ZB lattice; Γ has both X and Γ points folded in. It is evident that there is a pronounced bowing at both Γ and L, as also shown in Fig. 4, where we report the QS*GW* bandgap as function of Ge concentration.

Figure 5 summarizes the relationship between DFT (a, lattice constant) and QS*GW* (E_G, bandgap). From left to right, we report the bandgap for Ge, **III**, **IIb**, **IIa**, **I**, and pure GaAs. Once more we note the marked discontinuity for **IIb** from the general trend.

We finally remark on the lack of definitive analysis of the state of the alloy. In particular, the validity of two viewpoints, a probabilistic growth model based on a layer-by-layer deposition that rejects high-energy bond

Table 4 QS*GW* bandgaps for Γ and R in ordered $(GaAs)_{1-x}Ge_{2x}$ alloys

	Γ	R
GaAs	1.66	1.80
I ($x = 0.25$)	0.61	0.20
IIa ($x = 0.5$)	0.16	−0.41
IIb	<0	<0
III ($x = 0.75$)	0.23	−0.18
Ge	1.04	0.74

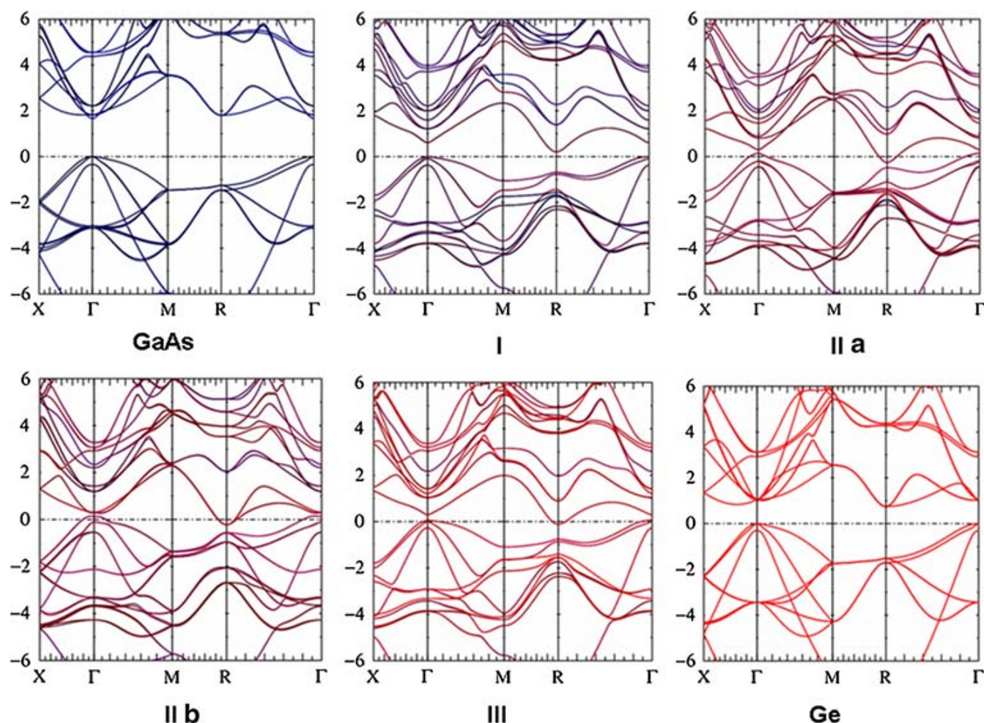

Fig. 3 Electronic structure for the considered systems, GaAs (*first, left up*), Ge (*last, right bottom*), and the four intermediate alloys **I, IIa, IIb, III**

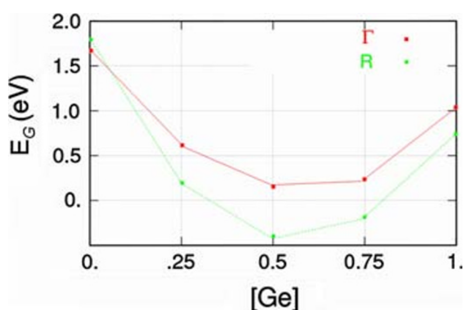

Fig. 4 QS*GW* calculated bowing of the bandgap at Γ and *R* versus different concentration of Ge atoms

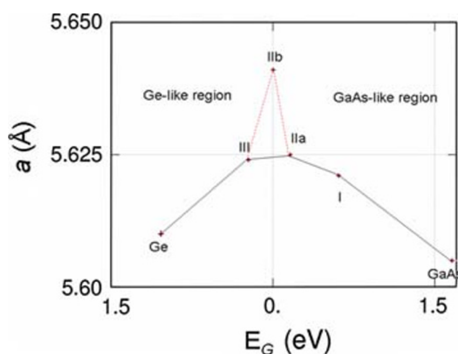

Fig. 5 From left to right: Ge → alloys → GaAs bandgaps calculated at the QS*GW* level versus lattice constant calculated at the PAW/LDA level (a_{calc}, from Table 3)

formation (As–As, Ga–Ga) [22] and a thermodynamic equilibrium based on an effective Hamiltonian (but which is able to describe electronic states [63]) needs to be assessed. In thermodynamic models [19], the Boltzmann weight can always be realized regardless of the measurement time; in probabilistic models [21, 22] further equilibration after the atomic deposition is not possible. It is apparent from the results of Figs 4 and 5 that our theoretical alloy models, and optical properties in particular, depend sensitively on the arrangement of atoms in the alloy.

Conclusions

We have focused on the class of $(\text{III–V})_{1-x}\text{IV}_{2x}$ alloys, as candidate new materials with applications relevant to photovoltaics. Previous experiments reported an asymmetric (nonparabolic) bowing of the bandgap as a function of the concentration of the III–V and IV constituents in the alloy.

We have built and optimized 8-atom $(\text{GaAs})_{1-x}\text{Ge}_{2x}$ ordered compounds, with x ranging from 0 to 1, as elementary models of alloys. For these systems, we have thus employed DFT to determine structural properties and reaction energies, and QS*GW* to study optical properties. For the more diluted and more concentrated Ge models, **I** and **III**, we have predicted stabilizing clustering effects accompanied by a lowering of the products–reactants excess energy. These two systems are symmetric and additionally characterized by an almost identical lattice parameter. In other words, the calculated excess energy of the two intermediate models (**IIa** and **IIb**, $x_{\text{Ge}} = 0.5$),

clearly showed that the octet rule violation has lead to the final instability of the alloys. In particular, the larger the number of III–IV and IV–V bonds, the larger the instability of the model. We detected a linear relationship between formation energy and number of bad bonds in the alloys. The relevance of this result stems by the fact that for stoichiometric compounds an elementary model Hamiltonian for the energetics of any alloy with equal numbers of Ge cations and anions as function of the number of bad bonds can be developed.

Our QS*GW* calculations confirm the bowing of the alloy both at the Γ and *L* points. We also detected direct relationships between optical and mechanical properties: a diminished cohesion for the intermediate alloys (**IIb** is even almost metallic), with a sensitive reduction in the bandgap was clearly coupled with an increase in lattice parameter and with a reduced symmetry of these two structures. The reduction in symmetry for the intermediate alloys is also considered the fingerprint of an ordered–disordered phase transition for our alloy models.

Acknowledgments This research was supported by a Grant from KAKENHI (#21245004) and the Global COE Program [Chemical Innovation] from the Ministry of Education, Culture, Sports, Science, and Technology of Japan.

Open Access This article is distributed under the terms of the Creative Commons Attribution Noncommercial License which permits any noncommercial use, distribution, and reproduction in any medium, provided the original author(s) and source are credited.

References

1. C. Kittel, *Introduction to Solid State Physics* (Wiley, New York, 2005)
2. M. Levinstein, *Handbook Series on Semiconductor Parameters vol 1, 2* (World Scientific, London, 1999)
3. S.Q. Wang, H.Q. Ye, J. Phys.: Condens. Matter **14**, 9579 (2002)
4. B.G. Streetman, S. Banerjee, *Solid State electronic Devices* (Prentice Hall, New Jersey, 2000)
5. H. Holloway, Phys. Rev. B **66**, 075131 (2002)
6. K.E. Newman, J.D. Dow, B. Bunker, L.L. Abels, P.M. Raccah, S. Ugur, D.Z. Xue, A. Kobayashi, Phys. Rev. B **39**, 657 (1989)
7. R. Osorio, S. Froyen, Phys. Rev. B **47**, 1889 (1993)
8. A.G. Rodriguez, H. Navarro-Contreras, M.A. Vidal, Phys. Rev. B **63**, 115328 (2001)
9. T. Ito, T. Ohno, Surf. Sci. **267**, 87 (1992)
10. T. Ito, T. Ohno, Phys. Rev. B **47**, 16336 (1993)
11. K.E. Newman, D.W. Jenkins, Superlattices and Microstruct **1**, 275 (1985)
12. M.A. Bowen, A.C. Redfield, D.V. Froelich, K.E. Newman, R.E. Allen, J.D. Dow, J. Vac. Sci. Technol. B **1**(3), 747 (1983)
13. S.A. Barnett, M.A. Ray, A. Lastras, B. Kramer, J.E. Greene, P.M. Raccah, L.L. Abels, Electron. Lett. **18**, 891 (1982)
14. Zh.I. Alferov, M.Z. Zhingarev, S.G. Konnikov, I.I. Mokan, V.P. Ulin, V.E. Umanskii, B.S. Yavich, Sov. Phys. Semicond. **16**, 532 (1982)
15. A.G. Norman, J.M. Olson, J.F. Geisz, H.R. Moutinho, A. Mason, M.M. Al-Jassim, M. Vernon, Appl. Phys. Lett. **74**, 1382 (1999)
16. I. Banerjee, D.W. Chung, H. Kroemer, Appl. Phys. Lett. **46**, 494 (1985)
17. A.J. Noreika, M.H. Francombe, J. Appl. Phys. **45**, 3690 (1974)
18. S.H. Baker, S.C. Bayliss, S.J. Gurman, N. Elgun, J.S. Bates, E.A. Davis, J. Phys.: Condens. Matter **5**, 519 (1993)
19. K.E. Newman, J.D. Dow, Phys. Rev. B **27**, 7495 (1983)
20. A.G. Rodriguez, H. Navarro-Contreras, M.A. Vidal, Appl. Phys. Lett. **77**, 2497 (2000)
21. E.A. Stern, F. Ellis, K. Kim, L. Romano, S.I. Shah, J.E. Greene, Phys. Rev. Lett. **54**, 905 (1985)
22. K. Kim, E.A. Stern, Phys. Rev. B **32**, 1019 (1985)
23. L.C. Davis, H. Holloway, Phys. Rev. B **35**, 2767 (1987)
24. H. Holloway, L.C. Davis, Phys. Rev. B **35**, 3823 (1987)
25. H. Holloway, L.C. Davis, Phys. Rev. Lett. **53**, 830 (1984)
26. M.I. D'yakonov, M.E. Raikh, Fiz. Tekh. Poluprovodn. **16**, 890 (1982). Sov. Phys. Semicond. 16, 570 (1982)
27. K. Mader, A. Zunger, Phys. Rev. B **51**, 10462 (1995)
28. Y. Seong, A.G. Norman, I.T. Ferguson, G.R. Booker, J. Appl. Phys. **73**, 8227 (1993)
29. J.P. Perdew, A. Zunger, Phys. Rev. B **23**, 5048 (1981)
30. D.M. Ceperley, B.I. Alder, Phys. Rev. Lett. **45**, 566 (1980)
31. K. Burke, J.P. Perdew, *Y. Wang* (Electronic Density Functional Theory: Recent Progress and New Directions, Plenum Press, New York, 1998)
32. J.P. Perdew, *Electronic Structure of Solids 91* (Akademie Verlag, Berlin, 1991)
33. J.P. Perdew, J.A. Chevary, S.H. Vosko, K.A. Jackson, M.R. Pederson, D.J. Singh, C. Fiolhais, Phys. Rev. B **46**, 6671 (1992)
34. P.E. Blöchl, Phys. Rev. B **50**, 17953 (1994)
35. G. Kresse, D. Joubert, Phys. Rev. B **59**, 1758 (1999)
36. M. Methfessel, M. van Schilfgaarde, R. A. Casali, Electronic Structure and Physical Properties of Solids: The Uses of the LMTO Method, Lecture Notes in Physics 535, 114.(Springer-Verlag Berlin 2000)
37. L. Hedin, Phys. Rev. **139**, A796 (1965)
38. R. Gomez-Abal, X. Li, M. Scheffler, C. Ambrosch-Draxl, Phys. Rev. Lett. **101**, 106404 (2008)
39. T. Kotani, M. van Schilfgaarde, Solid State Commun. **121**, 461 (2002)
40. T. Kotani, M. van Schilfgaarde, S.V. Faleev, Phys. Rev. B **76**, 165106 (2007)
41. M. van Schilfgaarde, T. Kotani, S.V. Faleev, Phys. Rev. B **74**, 245125 (2006)
42. M. van Schilfgaarde, T. Kotani, S.V. Faleev, Phys. Rev. Lett. **96**, 226402 (2006)
43. M. Shishkin, M. Marsman, G. Kresse, Phys. Rev. Lett. **99**, 246403 (2007)
44. A.N. Chantis, M. van Schilfgaarde, T. Kotani, Phys. Rev. Lett. **96**, 086405 (2006)
45. L. Viña, S. Logothetidis, M. Cardona, Phys. Rev. B **30**, 1979 (1984)
46. P. Lautenschlager, M. Garriga, S. Logothetidis, M. Cardona, Phys. Rev. B **35**, 9174 (1987)
47. C.Y. Yeh, Z.W. Lu, S. Froyen, A. Zunger, Phys. Rev. B **46**, 10086 (1992)
48. S.Q. Wang, H.Q. Ye, J. Phys.: Condens. Matter **15**, L197 (2003)
49. S. Kalvoda, B. Paulus, P. Fulde, Phys. Rev. B **55**, 4027 (1997)
50. K.H. Hellwege, O. Madelung, *Landolt–Börnstein New Series Group III* (Springer, Berlin, 1982)
51. J. Singh, *Physics of Semiconductors and their Heterostructures* (McGraw & Hill, New York, 1993)
52. H. Arabi, A. Pourghazi, F. Ahmadian, Z. Nourbakhsh, Phys B: Condens Matter **373**, 16 (2006)
53. A. Wronka, Mater Sci-Pol **24**, 726 (2006)
54. CRC Handbook of Chemistry & Physics, (1997-1998)
55. M. Murayama, T. Nakayama, Phys. Rev. B **49**, 4710 (1994)
56. A. Bautista-Hernandez, L. Perez-Arrieta, U. Pal, J. F. Rivas Silva, Rev. Mex. Fis. **49**, 9 (2003)

57. G. Henkelman, A. Arnaldsson, H. Jónsson, Comput. Mater. Sci. **36**, 354 (2006)
58. E. Sanville, S.D. Kenny, R. Smith, G. Henkelman, J. Comp. Chem. **28**, 899 (2007)
59. W. Tang, E. Sanville, G. Henkelman, J. Phys.: Condens. Matter **21**, 084204 (2009)
60. S. Zhang, J. Northrup, Phys. Rev. Lett. **67**, 2339 (1991)
61. L. Landau, Zh. Eksp. Teor. Fiz. **7**, 19 (1937)
62. T. Mattila, R.M. Nieminen, Phys. Rev. B **54**, 16676 (1996)
63. Y. Bar-Yam, D. Kandel, E. Domany, Phys. Rev. B **41**, 12869 (1990)